Methodology for Modeling Detailed Imperfect Mixing Effects in Complex Reactors

Gary J. Wells and W. Harmon Ray
Dept. of Chemical and Biological Engineering, University of Wisconsin–Madison, Madison, WI 53706

DOI 10.1002/aic.10407
Published online April 4, 2005 in Wiley InterScience (www.interscience.wiley.com).

A powerful new modeling technique is presented for exploring mixing effects in reactive flow systems. The technique combines the detailed mixing representation of computational fluid dynamics (CFD) simulations with the simplicity and computational efficiency of stirred-tank compartment models. The method can be generally applied to many reactive systems, and requires only that appropriate criteria be specified to select compartment models from a single converged CFD simulation. A 1000-fold increase in computational speed is achieved by the new compartment model/CFD technique when modeling steady-state operation of low-density polyethylene (LDPE) autoclave reactors, making broad studies of operating conditions and stability possible. Results from compartment models are shown to capture the accuracy and detail of CFD simulations over a wide range of LDPE reactor operation, and the new technique provides a combination of modeling detail and computational ease not previously available for this type of reactor. © 2005 American Institute of Chemical Engineers *AIChE J,* 51: 1508–1520, 2005
Keywords: mixing, compartment models, computational fluid dynamics, low-density polyethylene, autoclave reactor

Introduction

Mixing can play a substantial role in determining the overall productivity, stability, and operability of reactive systems. Recent advances in computational fluid dynamics (CFD) provide promise for detailed modeling of imperfect mixing and reaction. However, CFD can be computationally intensive, and simpler techniques such as compartment models have been widely used to understand imperfect mixing in reactive systems. It is therefore attractive to apply detailed mixing knowledge from CFD in tandem with such simpler techniques. One approach achieves this combination by determining individual model parameters such as flow or diffusion constants from nonreactive CFD simulations and subsequently applying them to simpler reactive models.[1,2] A more general approach, however, is to integrate fully reactive CFD models directly in process simulation studies or as computationally efficient reduced models.

The integration of mixing details obtained from CFD in computationally efficient process simulations would allow researchers to explore detailed mixing effects in a variety of new ways. For instance, a detailed representation of a reactor could feasibly be embedded into a larger flow sheet model that involves units upstream and downstream of the reactor. Additionally, the effects of detailed flow, temperature, and composition fields could be addressed efficiently in the context of other simulation methods. Possible applications of such a combined approach include continuation and stability analysis, controller design, or modeling of complex product distributions such as those resulting from polymerization.

Several important efforts have been made to address different aspects of the general task of combining CFD-level detail into more traditional chemical process models. The *network-of-zones model* of Mann and coworkers[3-6] applies an efficient zonal model to simulate reactive flow fields. Their approach is quite general in nature, and it is typically implemented using zones with shapes and volumes chosen a priori based on some

Correspondence concerning this article should be addressed to W. H. Ray at ray@engr.wisc.edu.

information about the flow field character. As a result of this scheme, thousands of control volumes are often needed to solve the reactive field. Such models, although faster than their full reactive CFD counterparts, are still computationally intensive. This limits their use in the study of steady-state stability over wide operating ranges.

Osawe et al.[7] applied an approach to combine simulations generated using the Fluent CFD package[8] with the Aspen process flow sheet modeling package (AspenTech). Their approach either integrates Fluent flow models in their full complexity into Aspen or uses a multidimensional interpolation technique to obtain needed values from a database of precomputed steady-state CFD results. Bezzo et al.[9] developed a framework that integrates CFD models in their full form inside of the gPROMS process simulation environment.[10,11] This approach allowed the Fluent CFD package[8] to compute the momentum balances and quantities such as heat-transfer coefficients, whereas the process simulator computed the larger flow-sheet simulations. Further work along these lines by Bezzo et al.[12] presents a general approach for determining flow quantities from nonreactive CFD simulations and applying them in zonal reaction models of bioreactors. Flow parameters such as the fluid viscosity and shear rate dominate the reaction rate for the case modeled by Bezzo et al.,[12] and these flow parameters were the primary variables used to select zonal volumes and parameterize the reactive model. Spatial segregation of temperature or composition was not considered in either their CFD modeling or their selection of zonal volumes.

The existing approaches in the literature have illustrated how the integration of CFD flow simulations with larger flow-sheet models provides substantial benefits in process design. However, process stability has not been considered using such methods. Further, to accurately describe situations in which spatial segregation of composition and temperature greatly influence reaction, an alternative approach to combining mixing details from reactive CFD with simplified models may be advantageous. Such a method may be especially useful in prediction of the behavior of polymerization processes that depend highly on spatial variations in the reaction environment.

This work addresses the task of integrating mixing details into process models that are both simple to compute and have the ability to accurately assess a wide range of operating conditions. A method of selecting simplified compartment models from reactive CFD simulations is presented, and this method is applied to a complex case study involving production of low-density polyethylene (LDPE) in a stirred autoclave reactor. Mixing effects in this process influence not only productivity and initiator effectiveness,[13-16] but also stability and product properties.[17,18] Using this example, a sampling of the advantages provided by the CFD/compartment model approach is illustrated. General guidelines are also given for applying the new approach to other classes of reactive flow systems where detailed composition and temperature fields have a substantial influence on reaction.

Low-Density Polyethylene Reactors

In this work, simulation studies are applied to describe behavior of an LDPE autoclave reactor with a design similar to that used industrially (see schematic in Figure 1). LDPE is an important commodity polymer that accounts for about a quarter

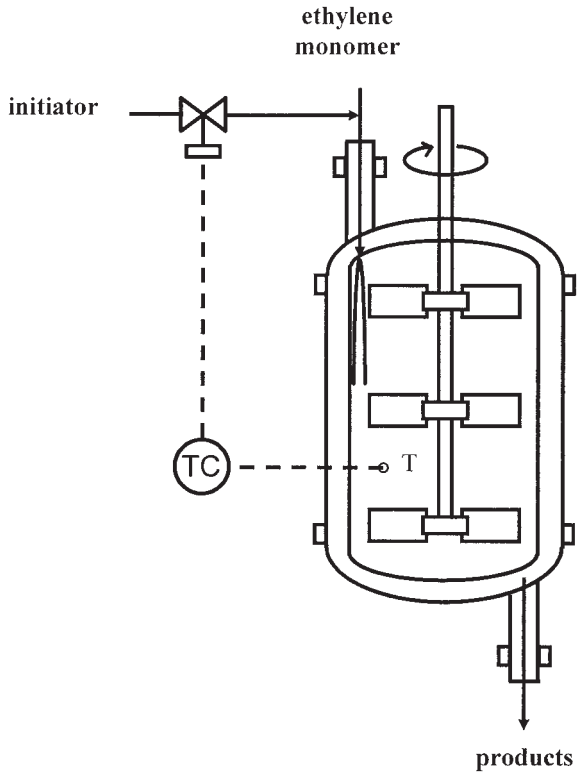

Figure 1. View of the LDPE autoclave reactor.

of the U.S. production of polyethylene.[19] Typical operation in these reactors involves high pressures (1500–2500 bar), high temperatures (200–300°C), and short residence times on the order of 10 s to 1 min. The volume of autoclave reactors ranges from about 250 to 2000 L. The heat generated by polymerization is quite high and causes a temperature rise of about 12–13°C for each percent of monomer conversion.[20] Because of relatively short residence times and thick reactor walls, the capability of removing heat through wall cooling is quite low.[21] Thus, autoclave reactors can be considered adiabatic, and the temperature increase is solely attenuated by feeding the monomer at low temperatures.[22] As a consequence of safety limits on the maximum temperature rise and the low residence times, conversion in autoclave reactors is usually $<20\%$. At temperatures $\gtrsim 310$°C, a violently exothermic reaction can decompose ethylene, leading to localized dark spots in the polymer or global reactor runaway.

In an attempt to achieve good mixing in the LDPE autoclave, agitation of the reactor contents is often quite intense, with an energy input of up to 100 kW/m^3 for stirring.[23] Despite this high degree of agitation, numerous researchers have indicated that imperfect mixing plays a significant role in the LDPE autoclave because of the similarity of reaction and mixing timescales.[13-18,25-27] For this reason, the LDPE autoclave reactor provides an excellent case study for development of detailed modeling techniques that capture imperfect mixing effects on reaction.

Reaction Kinetics

Table 1 presents the reactions constituting the kinetic mechanism used in this work for modeling free-radical ethylene

Table 1. Kinetic Mechanism for Free-Radical Homopolymerization of Ethylene

Initiation

$I \xrightarrow{f_{eff}k_d} 2R$ (decomposition of initiator)

$R + M \xrightarrow{\text{fast}} P_1$ (initiation of growing chain)

Chain propagation

$P_n + M \xrightarrow{k_p} P_{n+1}$

Termination by combination

$P_n + P_m \xrightarrow{k_{tc}} D_{n+m}$

*Ethylene decomposition**

$M \xrightarrow{C_{mon}(1.89k_{md1} + k_{pd1}) + 0.0714k_{pd2}}$ decomp products + 30,200 cal/mol

Note: Ethylene decomposition ("decomp") is modeled as a heat release only; decomp products are not explicitly tracked. This simplified form of the decomp model proposed by Zhang et al.[28] relates the rate of heat generation from monomer decomp to lumped kinetic parameters (k_{md}, k_{pd1}, k_{pd2}) from the decomposition mechanism as follows[29]

$$R_{heat,decomp} = \Delta H_{decomp}[C_{mon}^2(1.89k_{md} + k_{pd1}) + 0.0714k_{pd2}C_{mon}]$$

homopolymerization in the high-pressure autoclave reactor. As can be seen, the common free-radical initiation, propagation, and termination steps are modeled. In this work, *tert*-butyl perxoxyacetate (TBPOA) is used as the only initiator. This initiator is relatively active, with a half-life that is about 2 s at 200°C, but considerably shorter at higher temperatures. Radical termination is considered to occur exclusively by coupling because many researchers consider it to be the principal termination mechanism for LDPE.[30] Table 2 presents the rate constant parameters that are used in this study to define reactive source terms. These rate constants are assumed to be of the Arrhenius form, and both temperature and pressure dependencies are given in the table. A simplified form of the ethylene decomposition model proposed by Zhang et al.[28] is applied whereby only the heat release arising from the reaction is considered.[29]

Table 3. Constant Values Specified in This Work for Modeling the LDPE Autoclave Reactor*

Quantity	Value
Inlet flow velocity	50 m/s
Residence time	32.8 s
Impeller rotation rate	200 RPM
Reactor volume	500 L
Mixture density	499 g/L
Heat capacity	2.768 J g^{-1} K^{-1}
Species diffusivity	2.88×10^{-5} m^2/s
Heat conductivity	0.1998 J m^{-1} s^{-1} K^{-1}
Mixture viscosity	1.6×10^{-3} kg m^{-1} s^{-1}
Initiator efficiency	1
Reactor pressure	2000 atm
Heat of polymerization	−21,386 cal/mol
Heat of decomposition	−30,200 cal/mol

Note: Values for physical constants are taken from Read et al.[27]

Detailed Reactive Flow Modeling of the LDPE Autoclave Reactor Using CFD

CFD model setup and solution

To simulate the LDPE autoclave reactor, a commercial finite-volume CFD package (Fluent[8] version 6.0.2) is used. Constant values used in the simulations are given in Table 3. The reactor geometry, shown in Figure 2 with the CFD grid, is selected to represent a DuPont-type autoclave reactor with a length-to-diameter ratio of 2.5. The geometric features used in the autoclave reactor model are the same as those used by Read et al.[27] and are taken from the literature and patent sources. The total volume of the reactor is taken to be about 500 L, a capacity in the range of reported industrial operation. Two of the four impellers used in this model are tilted at 45 ° to allow for increased end-to-end mixing, a widely recognized way of improving reactor performance.[22]

The CFD reactor mesh used in this study is a structured, hexahedral, boundary-fitted grid. Increased grid density is placed in the region near the feed pipe to help capture the steep gradients in temperature and composition that can be experienced there. A total of about 100,000 grid cells is used for the entire reactor.

To solve for the turbulent flow field, the renormalization group (RNG) modification[34] of the k–epsilon (k–ε) turbulence model[35] is used. To handle the impeller rotation, a single rotating reference frame is employed, using the same simulation methodology used by Read et al.[27] The feed is assumed to be a thoroughly premixed stream composed only of ethylene monomer and initiator. The feed temperature and initiator feed

Table 2. Kinetic Parameters Used to Study the LDPE Autoclave*

Reaction	Units	k_0	E_A (cal/mol)	V_A (cal/atm-mol)	Source
Propagation (k_p)	L mol^{-1} s^{-1}	1.14×10^7	7091	−0.477	31
Initiator decomposition (k_d)	s^{-1}	1.06×10^{16}	35,560	0.0605	32
Termination by coupling (k_{tc})	L mol^{-1} s^{-1}	3.00×10^9	2400	0.3147	31
Initial monomer decomp. (k_{md})	L mol^{-1} s^{-1}	4.00×10^{19}	65,000	−0.1937	28
Decomp. propagation 1 (k_{pd1})	L mol^{-1} s^{-1}	1.59×10^{20}	65,000	0.3218	28
Decomp. propagation 2 (k_{pd2})	s^{-1}	4.39×10^{20}	65,000	−0.1937	33

*Rate constants (k) are computed using the formula: $k = k_0\exp[-(E_A + V_A \cdot P)/R_{gas}T]$, where P is the absolute pressure in atm, T is the absolute temperature in K, and R_{gas} is the ideal gas constant.

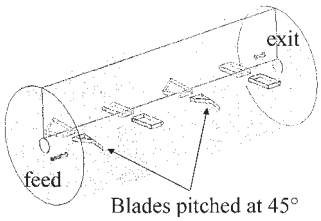

Figure 2. Overall view of CFD grid used for the LDPE autoclave reactor.

About 100,000 hexahedral grid cells are used. Reactor geometry is the same as that used by Read et al.,[27] and corresponds to a selection of industrially relevant design parameters published in the literature.

fraction are varied as parameters for study. Fluid properties are assumed to be independent of temperature and constant throughout the reactor volume.

To solve the complete CFD case with temperature, species, and radical concentration fields, a two-step process is used:

(1) The turbulent flow quantities and mean velocities are determined using the rotating reference frame.

(2) The flow field is fixed at the converged values, and the convective fluxes are internally converted to the stationary, nonrotating frame. These convective terms are then used to solve the transport equations for enthalpy, species mass fractions, and total radical concentration.

This two-step process saves significant computational time because of the reduced number of equations solved at each stage. As a result of the stagewise solution process, it is assumed that the flow field is not significantly affected by the reaction. This assumption is acceptable if: (1) density and viscosity changes are small in comparison to other effects, and (2) turbulent eddy dissipation and diffusion do not limit the reaction rate. The assumption of small viscosity and density variations can be justified by the low degree of conversion to polymer, common in LDPE autoclaves. Also, the viscosity is close to that of liquid water at the supercritical conditions of the reactor,[24] so viscous effects are generally not large. Justification for neglecting turbulent mixing and diffusion effects is treated in the next section.

Evaluation of possible turbulent mixing and diffusive effects on reaction

In the production of LDPE, total bulk polymer production and heat generation are governed by three core reaction mechanisms: initiator decomposition, propagation, and termination. As stated above, this work assumes that the rates of these reactions are controlled by reaction kinetics alone. As a consequence, it is assumed that the turbulent dissipation of eddies and molecular diffusion both occur on shorter timescales than the kinetic rates. For the decomposition of initiator, this assumption is warranted because the reaction is unimolecular, and no transport of species by diffusion or turbulent eddy dissipation is required for the reaction to take place. The propagation reaction between a growing free radical and a monomer molecule has a timescale about 1000th that of the growing chain lifetime. However, with low monomer conversion and very small growing chain (free radical) concentrations, the growing chain end has a huge surplus of monomer in the volume contained in its radius of gyration. This means that the growing chain can add thousands of monomer units without significantly reducing the local monomer concentration in its growth environment. Thus, the propagation rate will not be limited either by diffusion or turbulent eddy dissipation. Analysis of the final core reaction mechanism for LDPE—bimolecular termination—requires more in-depth consideration.

When various polymers are produced by free-radical kinetics, the *gel effect* (also termed the Trommsdorf effect) is known to significantly limit diffusion for the bimolecular termination reaction.[36] This phenomenon occurs at high polymer content where the active radical centers on large macromolecules cannot diffuse easily to meet each other and terminate. Thus, translational diffusion of the polymer chain controls the rate.

Although some researchers have chosen to apply a multiplicative, conversion-dependent gel effect parameter to limit the termination rate at high polymer content,[37] this effect is not considered herein. In the case of low-density polyethylene production in autoclave reactors, conversion is generally low (10–20%), and the gel effect is considered negligible under these conditions. For these reasons, diffusion limitations of the termination rate are not considered here.

Guidance concerning the effect of turbulent eddy dissipation can be obtained by comparing the relevant reactive timescales to the turbulent mixing timescale. The timescale for bimolecular termination is generally defined in terms of the growing radical lifetime

$$t_{live} = 1/(k_t \mu_0) \tag{1}$$

The radical lifetime (t_{live}) is the total radical concentration (μ_0) divided by its rate of termination, and represents the average timescale over which radicals are active in producing polymer. In this work, through simulation of the LDPE autoclave at a wide variety of conditions, it has been found that the chain lifetime generally varies in the range from about 0.05 to 0.2 s.

Determining the timescale for turbulent mixing in reactive systems can be quite complex. Because of this complexity, these turbulent mixing timescales are the subject of current research,[38,39] and numerous expressions have been defined in the literature to assess them.[40-44] Such turbulent mixing timescale measures are often determined in a semiempirical fashion and yield alternative expressions, depending on the measurements used to fit them or the underlying assumptions of the analysis.

One of the most commonly used timescales for assessing turbulent mixing is the engulfment time constant defined by Baldyga et al.[44]

$$t_e = 17.3(\nu/\varepsilon)^{0.5} \tag{2}$$

This measure of mixing time assumes the turbulent mixing rates are independent of concentration gradients, and it provides an order of magnitude approximation for comparison to kinetic rates. In the current study, the engulfment time constant was found to vary between 0.01 and 0.05 s based on the assumed kinematic viscosity (ν) and the calculated CFD results for the turbulent eddy dissipation rate (ε). On the basis of this result, it is expected that the turbulent eddy dissipation rate would be somewhat faster than the rate of termination over the

operating range considered. Although there are some conditions under which the engulfment time is predicted to be in the same range as the radical lifetime, this situation generally occurs at temperatures on the high end of normal operating conditions (>270°C). At such operating conditions, the assumptions used in this study may not strictly hold, but they are not expected to introduce significant errors. This assessment of turbulent mixing timescales is in general agreement with CFD analysis of Tosun and Bakker[37] for modeling of the LDPE autoclave reactor. Their study, which incorporated experimentally determined flow boundary conditions, also showed that the mixing timescale is shorter than the reaction timescale for termination.

Convergence criteria and grid independence

To ensure that well-defined steady-state solutions were obtained from CFD simulations, convergence criteria that minimize the normalized errors of the velocity and scalar equations were selected to be more stringent than the default values suggested by the Fluent CFD software documentation.[8] Also, the temperature rise for converged solutions was determined to be within 0.01 K of the adiabatic rise resulting from the heat generation over the reactor volume from polymerization and monomer decomposition. Additionally, convergence criteria were adopted to ensure that cumulative errors in the overall reactor balances from inlet to outlet were small for each scalar quantity (enthalpy, species, radical concentrations). Grid independence was ensured by placing many grid cells in areas of high concentration and temperature gradients near the feed, and also by confirming the results using test cases with approximately double the grid cell density.

Generalized Compartment Models

In addition to CFD simulation, this work also explores the use of more traditional compartment model techniques to maintain computational simplicity and widen the feasible range of model application. In general, compartment models are used to capture imperfect mixing effects by simulating an entire reactor as several interconnected, idealized zones. These idealized zones are typically chosen to be well-stirred tanks or tubular reactors.[39,45]

The current work applies compartment models that consist of interconnected, perfectly mixed tanks. Such compartment models have been used extensively to approximate imperfect mixing patterns for various purposes. Example processes that have been examined using such compartment models include catalytic fluidized beds,[46] polymerization in vessel reactors,[14-18,47-49] and bioreactors.[4,12,50] Typically, these compartment models have only a small number of zones with relatively few parameters that are chosen using process knowledge.

Applicability of the generalized CFD/compartment modeling methodology for reactive flows

Before presenting the generalized CFD/compartment modeling methodology for reactive flows, it is important to state the limitations and assumptions behind the method. In this way, the classes of problems to which the method applies are distinguished from problems to which the method does not apply. Listed below are the two major assumptions of the method:

(1) *The reaction does not significantly affect the flow field, although the converse effect can be very significant*. This assumption implies that the fluid viscosity and density do not change significantly with reaction. In addition, the assumption is most likely to hold for nearly incompressible fluids with lower viscosity.

(2) *All significant reaction rates are determined by chemical kinetics*. This assumption implies that molecular diffusion and micromixing effects on the subgrid scale (such as turbulent eddy dissipation) do not limit reaction rate. Equivalently, this means that fluid motion influences reaction only through convective action. These assumptions are most likely to hold in reactors with premixed feed materials and highly turbulent flow fields. This means that imperfect macromixing on a length scale larger than turbulent eddies can be represented with compartment models.

Although the preceding assumptions represent a significant limitation in the scope of the new compartment model/CFD approach, there are many cases in which careful use of the method can provide an accurate and efficient assessment of reactive mixing. Example cases include highly exothermic polymerization reactions, some chlorination reactors with thoroughly premixed feeds,[51,52] and other exothermic reactions in the liquid or supercritical phase. As discussed in earlier sections, the two assumptions above are likely to hold for the LDPE autoclave reactor, given that fluid properties are relatively constant (attributed to low conversion), and the highly turbulent flow field present has micromixing timescales that are shorter than the important reaction kinetic timescales.

Formulation of the compartment models

In formulating the compartment models for this work, the terms of the general scalar equation of change must be enumerated for a single compartment that represents a particular reactor zone. Consider an assembly of compartments making up an industrial reactor such as that shown in Figure 3. Based on the assumptions of the previous section, the equation of change for the jth scalar quantity in compartment k, ϕ_j^k, can be written as

$$\frac{\partial \phi_j^k}{\partial t} = F_j^k + R_j^k \tag{3}$$

Here, F_j^k represents convective flow terms and R_j^k represents reactive source terms. Under the assumptions of this method, the reaction term R_j^k is the kinetic rate of change of the scalar quantity ϕ_j^k that would occur if the zone k were a batch reactor, and is thus governed only by the conditions in the region of interest. For perfect mixing in each zone k, the reaction term can be written as the sum of contributions from multiple reactions as follows

$$R_j^k = \sum_{i=1}^{N_{rxn}} R_{j,i}^k(\bar{\phi}^k) \tag{4}$$

where $\bar{\phi}^k$ is a vector representing the volume average values of the scalars in compartment k. The quantity R_j^k is the volume-averaged rate of production that occurs in the zone, and the

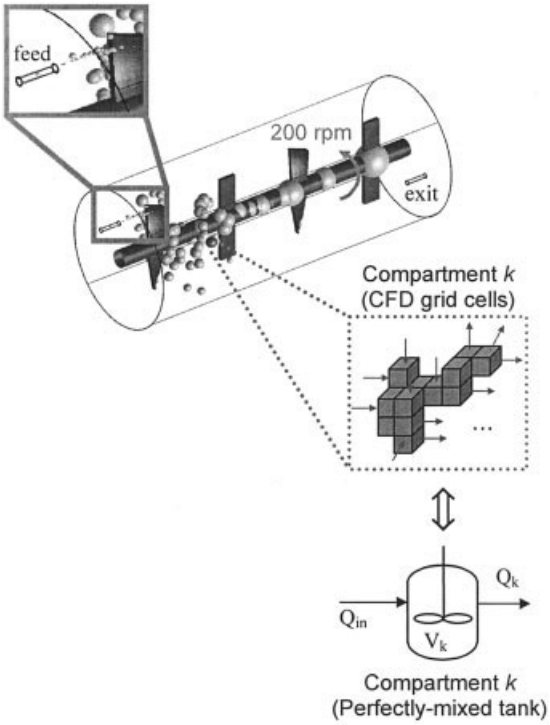

Figure 3. Perfectly mixed tank compartments selected from a CFD simulation.

The spheres shown here represent the compartments and are located at the centroids of the zones they represent. The volumes of the spheres are 1/8th that of the true tanks in the compartment model.

sum on the right-hand side of Eq. 5 is the net kinetic rate of change of ϕ_j^k (from all reactions) that would occur if the entire zone was uniform at the volume average conditions $\bar{\phi}^k$. Equation 5 is therefore exact if the zone in question is perfectly mixed, and is an approximation if the zone has some degree of spatial variation in temperature or composition. The units of R_j^k are expressed in mass terms if the quantity ϕ_j^k is a species weight fraction or enthalpy, and is expressed in molar terms if ϕ_j^k is a molar concentration.

Under the assumption that diffusion of scalar quantities in and out of the zone is small in comparison to convective transport, the only remaining term to define in Eq. 3 is the flow contribution F_j^k. The inflow to compartment k (Q_{in}^k) is composed of outflows from all neighboring compartments and possibly all or part of the main inlet flow:

$$Q_{in}^k = \sum_{n=0;n\neq k}^{N_{comp}} f_n^k Q_n \tag{5}$$

where Q_k is the total mass flow rate out of compartment k and f_n^k is the fraction of the outflow from compartment n that enters compartment k. The overall external feed to the reactor is represented by $n = 0$.

For an intensive scalar quantity ϕ_j^k, that is *per unit volume*, the following equation represents the convective flow term for perfectly mixed, constant volume tanks

$$F_j^k = \frac{1}{V_k}\left(\sum_{n=0;n\neq k}^{N_{comp}} f_n^k \frac{Q_n}{\rho_n}\bar{\phi}_j^n - \frac{Q_k}{\rho_k}\bar{\phi}_j^k\right) \tag{6}$$

where V_k and ρ_k are the total volume and density in compartment k, and F_j^k is the net flow rate of quantity j into and out of compartment k divided by the compartment volume. If we require that $f_k^k = -1$, then Eq. 6 can be written as follows

$$F_j^k = \frac{1}{V_k}\left(\sum_{n=0}^{N_{compt}} f_n^k \frac{Q_n}{\rho_n}\bar{\phi}_j^n\right) \tag{7}$$

To distinguish mass-based quantities from their volume-based counterparts, a circumflex (^) is used to denote mass-based quantities. The vector quantity $\bar{\phi}^k$ used earlier includes both mass-based and volume-based quantities. For an intensive scalar $\hat{\phi}_j^k$ that is *per unit mass*, the appropriate flow rate weighting is the mass flow rate Q_n. In this case, the flow source term for perfectly mixed zones is defined as

$$\hat{F}_j^k = \frac{1}{\rho_k V_k}\left(\sum_{n=0}^{N_{compt}} f_n^k Q_n \bar{\hat{\phi}}_j^n\right) \tag{8}$$

Here, $\hat{F}_j^k$ is the net flow rate of quantity j in and out of compartment k divided by the mass of material in that compartment.

In formulation of compartment models, it is not possible to independently specify the flow rates Q_n and the flow fractions f_n^k. At steady state, these flow rates and flow fractions are related by mass balances as follows

$$\mathbf{F}\mathbf{q} = -Q_0\mathbf{f}_0 \tag{9}$$

where

$$\mathbf{F} = \begin{bmatrix} f_l^1 & \cdots & f_{N_{compt}}^1 \\ \vdots & \ddots & \vdots \\ f_1^{N_{compt}} & \cdots & f_n^{N_{compt}} \end{bmatrix}; \quad \mathbf{q} = \begin{bmatrix} Q_1 \\ \vdots \\ Q_{N_{compt}} \end{bmatrix}; \quad \mathbf{f}_0 = \begin{bmatrix} f_0^1 \\ \vdots \\ f_0^{N_{compt}} \end{bmatrix}$$

and the overall external mass feed rate to the reactor is Q_0.

In practice, only the total mass flow rate to the entire reactor (Q_0) and the flow fractions (f_n^k) are specified for a compartment model. The compartment exit mass flow rates Q_n are computed for the individual compartments ($n \geq 1$) by using the mass balance relationship given above. It should be noted that for all compartments $n \geq 1$ without outflows leaving through the main reactor exit stream, $\Sigma_{k=1}^{N_{compt}} f_n^k = 0$. For those compartments $n \geq 1$ with some portion of the outlet flow leaving through the main reactor exit stream, $\Sigma_{k=1}^{N_{compt}} f_n^k < 0$.

A major advantage of the above approach is that almost all other perfectly mixed tank compartment models exist as a subset of this generalized formulation. Also, as will be shown in the next section, this formulation contains physically relevant terms such as the flow fractions f_n^k and compartment volumes V_k that can be obtained in a straightforward way from CFD simulations.

Numerical solution of compartment models for the LDPE autoclave

Using the generalized compartment model formulation described above, steady-state mixing models for the LDPE autoclave reactor are solved. Substituting Eqs. 4 and 7 into Eq. 3 yields the following expression for the generic volume-based quantity ϕ_j^k in compartment k

$$\frac{d\phi_j^k}{dt} = \sum_{i=1}^{N_{rxn}} R_{i,j}^k(\bar{\phi}^k) + \frac{1}{V_k}\left(\sum_{n=0}^{N_{compt}} f_n^k \frac{Q_n}{\rho_n}\bar{\phi}_j^n\right) \tag{10}$$

The corresponding equation for mass-based quantities is

$$\frac{d\hat{\phi}_j^k}{dt} = \sum_{i=1}^{N_{rxn}} \hat{R}_{i,j}^k(\bar{\phi}^k) + \frac{1}{\rho_k V_k}\left(\sum_{n=0}^{N_{compt}} f_n^k Q_n \bar{\hat{\phi}}_j^n\right) \tag{11}$$

For the LDPE autoclave reactor model, the above equations are solved for the average quantities $\bar{\phi}^k$ in each zone. Mass-based quantities $\hat{\phi}_j^k$ that are computed are the enthalpy, initiator mass fraction, and polymer mass fraction. The volume-based quantity ϕ_j^k computed in the LDPE compartment model is the total radical concentration. Considering both mass- and volume-based quantities, the compartment model requires solving four equations per compartment when no additional moments of the molecular weight distribution are computed. These state equations (see the Appendix) are scaled by the initial state values to improve performance of the numerical methods. Kinetic rate expressions based on the mechanisms of Table 1 are applied to compute reaction terms in the appropriate units.

Several different analyses have been performed using the compartment models, including steady-state computations, dynamic simulations, and stability analysis.[53] When solving for a steady state, the NLEQ package for nonlinear equation systems[54] is used. The AUTO package[55] is used to perform continuation and stability analysis, and dynamic simulations are computed using the DASSL package for differential–algebraic equations.[56] These packages for performing the continuation analyses, steady-state solutions, and dynamic simulations were applied with no special modifications using numerical, full Jacobian approximation schemes. A method for computing the full molecular weight distribution at steady state can also be applied as an extension to the imperfect mixing framework, and is addressed in a separate article.[57]

Methodology for Combining CFD and Compartment Models

The general compartment model formulation of the flow terms given in Eqs. 7 and 8 allows for the representation of very complex flow fields if the appropriate compartment model topology and flow connectivity are chosen. This complex representation gives the general compartment model formulation the potential to reproduce the flow detail of CFD simulations. To capture the spatial details of mixing, the compartment locations, size, and flow connectivity are selected from a CFD simulation at a base set of operating conditions.

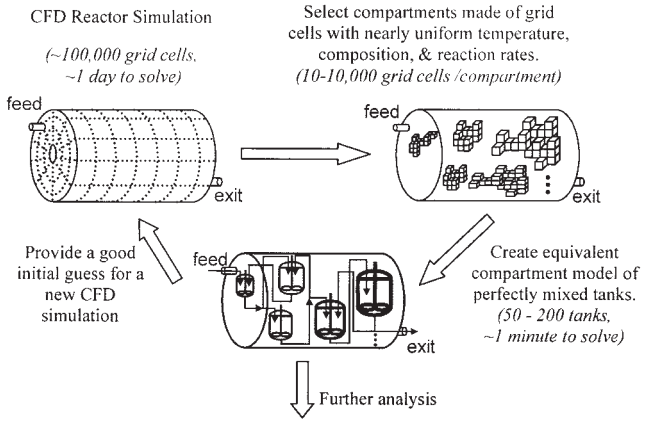

Figure 4. Procedure for selecting and using a compartment model.

Numerical values given in italics correspond to the specific case of the LDPE autoclave model.

Requirements for choosing accurate compartment models

Because compartment models follow the physical principles of mass and energy balances, they have the potential to extrapolate satisfactorily to operating conditions away from the base conditions. However, there are several criteria that must be met for the general compartment models to reproduce CFD results adequately over an extrapolated range of operating conditions. One of the major assumptions in the general compartment model formulation is that good mixing is present within each compartment. If there are large spatial variations in the conditions of a zone that is represented by a single compartment, it will be difficult for the compartment model to accurately capture the reaction and flow physics. Therefore, compartment models will extrapolate well to other conditions only if the zones represented by compartments remain well mixed.

Therefore, the first requirement in choosing a good compartment model is to select spatial regions that have small variations in temperature, species, and the important reaction rates. As a result, many compartments may be required to represent the detail of the species and energy fields, and the resulting models often contain more zones than traditional compartment models. Further, for the selected compartment model to extrapolate well, the general character of the flow field and the locations of gradients in composition and temperature must remain similar during extrapolation away from the base case. There are several factors that can change these quantities. First, if the reactor configuration, feed rate, or mixing rate changes, flow patterns can shift significantly, causing gradients to change locations. Second, large changes in density or viscosity may also cause the flow field and gradient locations to move. Additionally, if reactive timescales change significantly, the locations of temperature and species gradients can shift. However, if enough compartments are chosen to represent the reactor physics, compartment models can yield results that approximate a CFD solution while maintaining relative computational simplicity. This advantage of the compartment model technique will be illustrated in the next sections.

A conceptual view of the procedure used in this work to select compartment models from CFD is given in Figure 4.

Starting from a converged, CFD reactor simulation, spatial zones consisting of grid cells with nearly uniform temperature, composition, and reaction rates are selected. After these nearly uniform spatial zones are chosen, they are represented as perfectly mixed tanks in a compartment model. Each tank volume is computed by summing the volumes of the corresponding CFD grid cells that constitute the zone. Flows connecting the compartments are also determined from the CFD simulation through postprocessing of the converged results.

It should be noted that the procedure for selecting compartments can produce compartments of complex shapes that generally follow gradients in temperature and composition. Thus, this reduction method is more general in nature than coarsening of the CFD grid because CFD codes generally require grid cells of regular shapes such as hexahedra, tetrahedra, or prisms.[58]

Once the compartment model has been formulated, it can be used for a wide range of analyses. Because of the relative simplicity of the compartment models, they can be combined with continuation analysis techniques to quickly map the viable set of operating conditions. When predicting conditions that are far from the base CFD case, one can examine the inlet-to-outlet variations in temperature and composition for each compartment in the model to obtain an indication of the continued applicability of the simplified model. Large gradients across a single compartment may indicate that a new base CFD simulation should be used to generate a new compartment model.

Although these conditions should certainly be checked when performing simulations using the compartment models, it has been found that a single compartment model can be quite accurate over a wide operating range. Further, if required, compartment models can be used to provide a good initial guess for a CFD simulation at different conditions, thereby reducing the required computational time for convergence of the reactive CFD computation.

The complexity of the CFD and compartment models required to obtain accurate results will vary with the specific reactive case, as will the criteria for choosing compartments. The number of grid cells, compartments, and computational times for the LDPE autoclave simulations are given in italics in Figure 4. To illustrate more concretely how compartment models can be chosen from CFD, details related to modeling the LDPE autoclave will be presented in the next sections. However, it should be noted that adequate criteria for choosing compartments from CFD can be determined for any reactive system that satisfies the assumptions of the method, provided that enough compartments are included to subdivide the reactor into well-mixed zones. Further, the entire procedure for selecting compartment models has been automated in this work, and requires only that the criteria for choosing compartments be specified in advance. As will be shown in the next section, a single set of compartment selection criteria can be accurately applied for modeling a wide range of operating conditions.

Selecting a compartment model for the LDPE autoclave reactor

The first goal in choosing a good compartment model from a CFD simulation is to divide the reactor grid into portions that exhibit nearly perfect mixing. There are several ways to perform this subdivision, each with a different degree of success. In the case of the LDPE autoclave reactor simulations, a method has been chosen that sequentially divides and subdivides the reactor volume along CFD grid cell boundaries until a preset number of compartments is reached. After the subdivisions are completed, the flow and volume fraction parameters defined earlier are computed based on the zone volumes and interconnecting flow rates obtained directly from the CFD simulations.

The choice of criteria for subdividing the reactor is key to producing a good compartment model with the appropriate level of complexity. To accurately represent a zone as a perfectly mixed tank, the temperature, species concentrations, and all important reaction rates must be nearly uniform in the zone. Therefore, the criteria for choosing compartments for the LDPE autoclave model will focus on minimizing variations in the core kinetic rates, temperature, and composition. For the simulation work on the LDPE autoclave reactor, the two methods described below for subdividing the reactor volume have been used. These methods assume that the reactor is subdivided into a set of j grid cell groupings and the procedure starts with a single grouping containing all CFD grid cells.

(a) Reduction of the Variations of a Quantity ψ. For each of the current reactor grid cell groupings or subdivision (j), the maximum CFD grid cell value of ψ ($\psi_{\max,j}$) and minimum CFD grid cell value of ψ ($\psi_{\min,j}$) are stored. Then, the range of ψ is computed for each subdivision j: $\psi_{\max,j} - \psi_{\min,j}$. For the particular subdivision (k) that has the maximum range $\psi_{\max,k} - \psi_{\min,k}$, divisions are made into two parts. Grid cells in zone k with ψ above $\psi_{crit} = (\psi_{\max,k} + \psi_{\min,k})/2$ are grouped into one new subdivision. The remaining grid cells of zone k are grouped into another new subdivision. The total number of subdivisions increases by 1.

(b) Reduction of the Discrepancy between a Zone's Volume-Summed Kinetic Rate and the Rate That Would Occur at Average Conditions. For each grid cell i in a zone j, the value of some kinetic rate R_i^j is computed based on the localized temperatures and concentrations in cell i. Then, the sum of this rate over the individual grid cell volumes (the "true" total rate in the zone) is computed over the zone as follows

$$R_{true}^{tot,j} = \sum_{i=1}^{N_{cells}^j} R_i^j V_i \tag{12}$$

Note that R_i^j is a per-volume quantity, but $R_{true}^{tot,j}$ is not.

Next, for each zone j, the volume average values of temperatures and concentrations are computed. Then, the total rate *at these average zone conditions* is computed and multiplied by the zone volume, yielding a rate $R_{avg}^{tot,j}$ (not per-volume). Then, the zone k, which has the maximum absolute rate discrepancy $|R_{true}^{tot,k} - R_{avg}^{tot,k}|$, is selected for subdivision. All grid cells i in zone k with the grid cell kinetic rate

$$R_i^k > R_{crit} = \frac{1}{2}(R_{true}^{tot,k} + R_{avg}^{tot,k})\left[\sum_{i=1}^{N_{cells}^k} V_i\right]^{-1}$$

are placed into one new reactor subdivision. Those grid cells of zone k with $R_i^k < R_{crit}$ are placed into another new subdivision. The total number of subdivisions increases by 1.

Table 4. "Standard" 100-Compartment Model Selection Procedure for LDPE Autoclaves

(1) As a starting point, all CFD grid cells are considered to be in one subdivision of the reactor. This grouping of grid cells is subsequently divided and subdivided along grid cell boundaries.
(2) One of the reactor subdivisions is selected and further divided using method (a)* to reduce the *temperature variation* in the selected zone. This adds one subdivision.
(3) Step (2) is repeated 18 more times. After the initial division and the 18 repetitions, there are 20 reactor subdivisions.
(4) One of the reactor subdivisions is selected and further divided using method (b)* to reduce the *discrepancy of the propagation rate* in the selected zone. This adds one subdivision.
(5) One of the reactor subdivisions is selected and further divided using method (b)* to reduce the *discrepancy of the radical termination rate* in the selected zone. This adds one subdivision.
(6) The sequence of step (4) followed by step (5) is repeated 39 more times. After these repetitions, there are 100 reactor subdivisions.
(7) The final 100 zones for the compartment model are selected, and are represented as perfectly mixed tanks. The volumes of these tanks correspond to sum of the grid cell volumes in the zones they represent. The flows between tanks are the flows connecting the corresponding reactor zones.

Note: Methods (a) and (b) are described in detail in the previous section.

In this work, both of the subdivision methods (a) and (b) have been automated so that the procedure for compartment selection can be carried out quickly and easily. The compartment selection process typically takes about 1–2 min of computational time to complete on a current personal computer, most of which is required to simply read and parse the large amount of CFD data. It should be noted that neither of the methods presented above ensures that selected compartment zones are contiguous in space, but in practice the reactor subdivisions created using these methods are usually contiguous. Although the case of noncontiguous compartments may not be attractive in a conceptual sense, models with such compartments are still valid physical representations of the reactor if they are lumped and their respective volumes and interconnecting flows are correctly computed. More advanced methods of volume partitioning could be applied if spatially contiguous regions are strictly required.

For the LDPE autoclave, a "standard" set of criteria (sequence of divisions) was developed to generate a 100-tank compartment model from a CFD simulation. This "standard" set of criteria, summarized in Table 4, gives good results over a wide range of operating conditions. By attempting to choose zones that are nearly uniform in the temperature, propagation rate, and termination rate, the "standard" set of criteria tends to make the critical kinetic phenomena relatively uniform in the resulting compartments. This uniformity is achieved by choosing many small compartments in the region of the feed where high gradients in temperature and composition exist. More subtle gradients in downstream portions of the reactor are also captured. Figure 3, presented earlier, depicts the compartment locations and relative sizes for a typical 100-tank compartment model chosen for modeling the LDPE autoclave reactor. Although the specific choice of using 100 compartments is somewhat arbitrary in nature, it consistently provided for good compartment models that matched CFD results for this problem. In the next section of this work, compartment models created using the "standard" criteria are shown to represent the detailed mixing effects of CFD models.

Examination of Detailed Mixing Effects on the LDPE Autoclave Reactor

Figure 5 shows contour graphs through a plane intersecting the reactor impellers for a feed temperature of 360 K and an initiator feed fraction of 60 ppm of TBPOA. Temperature and radical concentration fields of the CFD solution are compared to those of a converged, 100-compartment model. The compartment model used in this case is based on the CFD run from the top portion of Figure 5, and was parameterized using the "standard" criteria given in Table 4. As can be seen in Figure 5, the compartment model matches the CFD results with a high degree of spatial detail for both contour graphs. These contours indicate that the compartment model accurately captures the effects of imperfect mixing in the LDPE autoclave at these conditions.

Figure 6 illustrates how the number of compartments influences the accuracy of the model when compared to CFD simulations. Results from CFD simulations are compared to those computed using continuation analysis of compartment models with 1, 15, and 100 tanks. Using the 120 ppm (feed initiator) CFD case as a basis, the 15-compartment model was chosen to minimize temperature gradients inside the selected zones, and the 100-compartment model was selected using the standard criteria of Table 4. The solid and dashed lines in Figure 6 represent stable and unstable branches for the compartment models. At 120 ppm of feed initiator, only the 100-compartment model predicts a stable operating point that is indicated by the detailed CFD simulations. Generally, the accuracy of the compartment models increases with the number of tanks in the model, and the 100-compartment model is capable of capturing the broadest range of operating conditions accurately. This good model performance arises from the physically relevant criteria used to define the 100-compartment model. Cases with a larger number of compartments (such as 200 tanks) do not show significant changes over 100-compartment models when similar selection criteria are used for the LDPE autoclave simulations. Other reactive flow systems may require fewer or more compartments to accurately replicate CFD results, depending on the complexity of temperature and composition fields and the sensitivity of key reaction mechanisms to imperfect mixing.

It should be noted that simulations presented here are performed only for operation near typical industrial conditions on the stable branch shown. There are additional solution branches corresponding to extinguished and runaway conditions, but detailed knowledge of operation on these branches is not necessary for the purposes of this discussion. Stability issues in the LDPE autoclave reactor are addressed in detail in a separate paper.[53]

Figure 7a further examines the degree of applicability of the 100-compartment models used in this study. The three curves shown in the figure are the results obtained from continuation analysis using a 100-tank model chosen based on the single, circled CFD run at $T_f = 420$ K and $w_{I,f} = 120$ ppm. Although the error incurred by extrapolating the 100-compartment model increases as the conditions become more remote from the base run, the basic trends are still well captured. The deviations are largest for the 300 K feed temperature curve. However, considering the large extrapolation of 120 K in feed temperature at this point, the results of the compartment model are quite good. In Figure 7b, compartment models are customized to the specific feed temperature examined, such that three base CFD

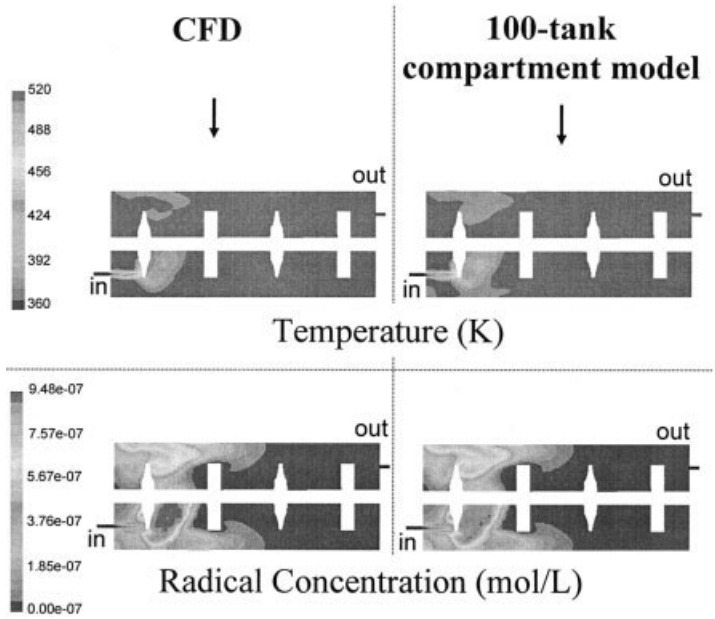

Figure 5. Comparison of CFD results to those from a 100-compartment model.

Both cases are for reactor operation with a feed temperature of 360 K and feed initiator fraction of 60 ppm TBPOA.

simulations are used to generate three 100-compartment models. In this case, the match of the compartment models to the CFD simulations is significantly improved for the lower feed temperatures of 360 and 300 K.

In addition to steady-state analysis, the compartment model/CFD approach can be accurately applied to dynamic simulations if the fluid physical properties and locations of temperature and composition gradients remain nearly constant during the transient period. For a simulation of a feed initiator fraction change, Figure 8 compares the time course of reactor exit temperature predicted by CFD to that computed using a 100-compartment model. It can be seen that the 100-compartment model matches the CFD results quite well over the entire transition period, even as the reactor moves away from the base conditions. This result indicates that the compartment model closely matches the mixing details of the CFD simulation during the transition. Further, the computational speed for running the dynamic 100-compartment model simula-

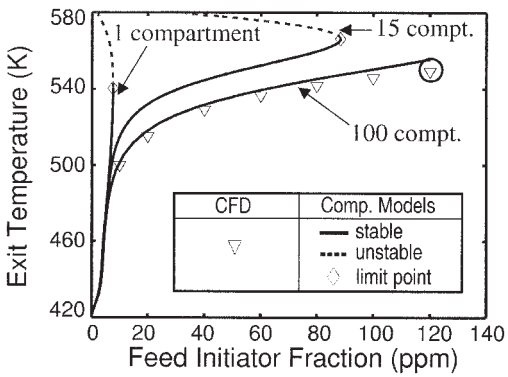

Figure 6. Comparison of CFD results to those of simpler zonal models.

The feed temperature is 420 K. The 15- and 100-compartment models were chosen based on the circled CFD run at a 120 ppm feed concentration of the initiator. The 15-compartment model was chosen to minimize temperature variations, and the 100-compartment model was chosen using the criteria of Table 4.

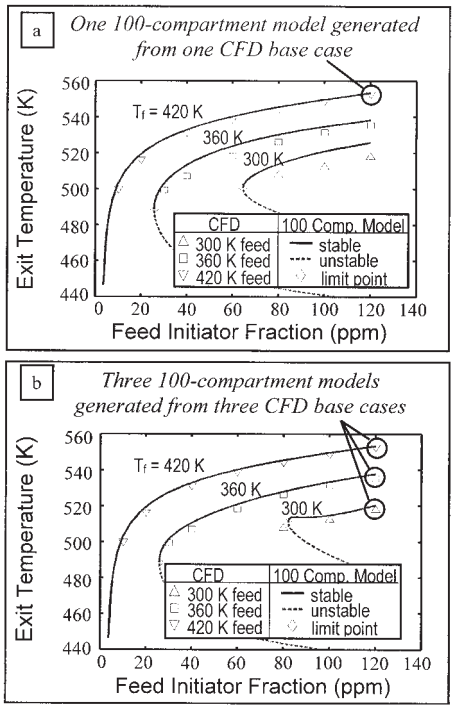

Figure 7. Applicability of compartment models over wide operating ranges.

Plots: (a) extrapolation of one compartment model in both feed temperature and initiator feed fraction, (b) extrapolation of three different models, each based on a single feed temperature

tion is about 70 times faster than an equivalent CFD simulation (see Table 5).

In general, better extrapolation of compartment models can be obtained by using more tanks in the models, as shown previously in Figure 6. However, the specific operating conditions of the CFD base case used to generate the compartment models also play a role in the accuracy at extrapolated conditions. If, at a base set of CFD conditions, the entire reactor volume is relatively uniform in temperature and reactive species, compartment models generated from this base set of conditions may not accurately predict poorly mixed reactor operation. The reason for this failure in extrapolation is that a well-mixed base CFD case has limited mixing information that can be used to determine the zonal volumes and locations of the compartment model. Conversely, if compartment models are selected from poorly mixed CFD base cases, they will easily represent reactor operation under well-mixed conditions, given that thoroughly mixed reactors can be accurately modeled with minimal spatial detail.

Benefits of the CFD/Compartment Model Approach

As illustrated in the previous section, compartment models of 100 interconnected, perfectly mixed tanks can accurately capture the spatial variations in temperature, conversion, and live chain concentrations found using complex CFD models. Furthermore, exit temperatures and polymer properties determined from such compartment models closely match CFD results. Because of the physical relevance of the compartment model parameters chosen, these models also satisfactorily match CFD results when extrapolated to operating conditions quite different from the base conditions.

The major advantage of these compartment models compared to CFD simulations is their relative computational simplicity. Table 5 shows the computational run times for various CFD and compartment model simulations. For computation of a single steady state after making a change of 20 ppm initiator feed, the compartment model takes about 1/2000 of the computational time required by CFD. Significant increases in computational speed are also achieved for dynamic simulations. Because nonoptimized, full Jacobian computation methods were applied during the zonal modeling stage, the speed benefit of the CFD/compartment model method is wholly derived from the reduction scheme.

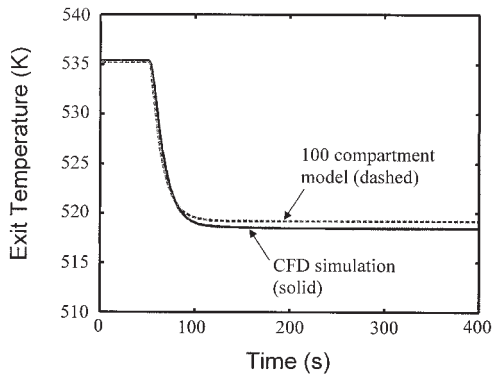

Figure 8. Predicted transient responses using CFD and a 100-compartment model.

Results are for dynamic simulations of an LDPE autoclave reactor operating at a feed temperature of 360 K originally at steady state for a feed initiator fraction of 120 ppm. A step change in the initiator feed fraction from 120 to 60 ppm is made at a time of 50 s. The 100-compartment model is chosen using the "standard" criteria of Table 4, based on the CFD simulation at a feed temperature of 360 K and initiator feed fraction of 120 ppm.

Table 5. Computation Times for a 100-Compartment Model and CFD Simulation

Item	CPU Time* (100-Tank Model)	CPU Time* (CFD)
Flow field	N/A	6 h
Reactive field from scratch	N/A	1 day
Reactive field, $\Delta w_{I,f} = 20$ ppm	15 s	12 h
Dynamic simulation, $\Delta w_{I,f} = 60$ ppm	10 min	12 h
Continuation curve	1 h	N/A

Computer: 1.33-GHz PC running Linux.

Because compartment models can be accurately extrapolated to new conditions, these models are excellent for determining the viable parameter space that can be explored. Examination of these operating conditions can therefore be efficiently achieved by using continuation analysis. For example, for a given feed temperature, simulations over the entire stable range of initiator weight fractions can be executed in only 1 h of computational time. This is nearly 20 times faster than a CFD simulation of the reactive field from scratch for just *one* initiator feed fraction. To compute an entire series of CFD solutions equivalent to the stable branch of a continuation analysis would depend on the spacing of the discrete points, and can take days of computation time to complete.

As computational power increases in the future, CFD will be increasingly applied to reactive flow problems. However, many problems suited to the new compartment model/CFD approach will still require long CFD computation times stemming from complex and spatially fine grids. For such complex cases, the methods developed in this work will remain useful in the future as an efficient method of exploring and analyzing wide operating ranges.

In addition to the advantages presented above, accurate compartment models can be used to obtain good initial guesses for CFD simulation at alternative operating conditions. Further, because these compartment models are relatively simple, it is also feasible to use them in optimization studies, controller design simulations, and dynamic simulations. Wider use of the method will be illustrated in additional articles focusing on stability[53] and the full product polymer molecular weight distribution[57] in LDPE autoclave reactors.

Acknowledgments

The authors are indebted to the industrial sponsors of the University of Wisconsin Polymer Reaction Engineering Laboratory and to the U.S. Department of Energy for financial assistance. We also thank Iasson Mustakis and Carlos Villa for their insight and support.

Notation

CFD = computational fluid dynamics
C_{mon} = monomer concentration, mol/L
C_p = heat capacity of mixture, cal g^{-1} K^{-1}

D_n = dead polymer chain of length n monomer units
E_A = activation energy used in the Arrhenius expression for rate constants, cal/mol
f_{eff} = effectiveness factor for initiator
f_n^k = fraction of exit flow from tank n that enters tank k. For $k = n$, this quantity is defined to be -1
f_0^k = fraction of the overall reactor feed stream (stream 0) that goes to tank k
F_j^k = flow term in the compartment model balance equation for a given volume-based quantity j in the compartment k
$\hat{F}_j^k$ = flow term in the compartment model balance equation for a given mass-based quantity j in the compartment k
k_o = preexponential factor for rate constants, variable units
k_d = rate constant for initiator decomposition, s^{-1}
k_{md} = rate constant for initial monomer decomposition, L mol^{-1} s^{-1}
k_p = rate constant for propagation, L mol^{-1} s^{-1}
k_{pd1} = rate constant for decomp propagation (path 1), L mol^{-1} s^{-1}
k_{pd2} = rate constant for decomp propagation (path 2), s^{-1}
k_{tc} = rate constant for termination by combination, L mol^{-1} s^{-1}
LDPE = low-density polyethylene
L/D = length-to-diameter ratio of reactor, dimensionless
M = monomer species
MW_{mon} = monomer molecular weight, g/mol
MW_I = initiator molecular weight, g/mol
N_{cells}^k = number of CFD grid cells in zone k
N_{compt} = number of compartments
N_{rxn} = number of reactions in kinetic mechanism
P = absolute pressure, atm
P_n = live polymer chain of length n monomer units
Q_o = overall inlet mass flow rate to the reactor, kg/s
Q_{in} = inlet flow rate, kg/s
Q_n = total mass flow rate leaving tank n to all destinations, kg/s
Q_{out} = outlet flow rate, kg/s
R_{gas} = ideal gas constant, 1.987 cal mol^{-1} K^{-1}
R = free radical
RNG = renormalization group
RPM = rotations per minute
R_i^j = a rate of reaction in cell i in zone j, mol L^{-1} s^{-1}
R_{crit} = critical value of rate used to determine reactor subdivisions, mol L^{-1} s^{-1}
$R_{heat,decomp}$ = rate of heat generation by monomer decomposition, cal L^{-1} s^{-1}
$R_{avg}^{tot,j}$ = total reaction rate at average conditions in zone j, mol/s
$R_{true}^{tot,J}$ = total reaction rate summed over grid cells in zone j, mol/s
R_j^k = rate of change of the jth generic scalar quantity in the compartment k
$R_{i,j}^k$ = rate source term for the jth generic scalar quantity in the compartment k for the ith reaction
T = local internal operating temperature, K
T_f = feed temperature, K
T^k = temperature in compartment k, K
TBPOA = *tert*-butyl peroxyacetate (peroxide initiator, 132.2 g/mol)
t_e = engulfment time, s
t_{live} = growing radical lifetime, s
V_A = activation volume, cal atm^{-1} mol^{-1}
V_{tot} = total reactor volume, L
V_i = volume of grid cell i, L
V_k = volume of compartment k, L
w_I^k = local initiator weight fraction in compartment k, dimensionless
w_p^k = local bulk polymer weight fraction in compartment k, dimensionless
$w_{I,f}$ = initiator feed fraction, ppm

Greek letters

ΔH_{poly} = heat of polymerization, cal/mol
ΔH_{decomp} = heat of decomposition, cal/mol
ε = rate of dissipation of turbulent eddies (distance^2/time^3 or energy mass^{-1} time^{-1})
μ_0 = total growing radical concentration, mol/L
μ_0^k = total growing radical concentration in compartment k, mol/L
ν = kinematic viscosity, m^2/s
ϕ_k^j = specific volume-based scalar quantity j in compartment k
$\hat{\phi}_k^j$ = specific mass-based scalar quantity j in compartment k
$\bar{\phi}^k$ = vector that denotes the average set of conditions in the zone k
ψ = a generic quantity
ψ_{crit} = critical value of a generic quantity used to subdivide the CFD grid into compartments
$\psi_{max,j}$ = maximum value of the generic quantity ψ in the jth subdivision
$\psi_{min,j}$ = minimum value of the generic quantity ψ in the jth subdivision
ρ = mixture density, g/L
ρ_n = density of the stream leaving tank n, g/L

Literature Cited

1. Vivaldo-Lima E, Wood PE, Hamielec AE, Penlidis A. Calculation of the particle size distribution in suspension polymerization using a compartment-mixing model. *Can J Chem Eng*. 1998;76:495-505.
2. Maggioris D, Goulas A, Alexopoulos AH, Chatzi EG, Kiparissides C. Prediction of particle size distribution in suspension polymerization reactors: Effect of turbulence nonhomogeneity. *Chem Eng Sci*. 2000; 55:4611-4627.
3. Mann R. Gas–liquid stirred vessel mixers: Towards a unified theory based on network of zones. *Trans IChemE*. 1986;64:23-34.
4. Zahradnik J, Mann R, Fialova M, Vlaev D, Vlaev SD, Lossev V, Seichter P. A networks-of-zones analysis of mixing and mass transfer in three industrial bioreactors. *Chem Eng Sci*. 2001;56:485-492.
5. Rahimi M, Mann R. Macro-mixing, partial segregation and 3-D selectivity fields inside a semi-batch stirred reactor. *Chem Eng Sci*. 2001;56:763-769.
6. Hristov HV, Mann R. Fluid mixing and the safe quenching of a runaway reaction in a stirred autoclave. *Trans IChemE*. 2002;80A:872-879.
7. Osawe M, Felix P, Syamlal M, Lapshin I, Cleetus KJ, Zitney SE. An integrated process simulation and CFD environment using the CAPE–OPEN interface specifications. Proc of AIChE Annual Meeting, Indianapolis, IN; 2002.
8. Fluent Inc. *Fluent User's Guide*, Version 6.0. Lebanon, NH: Fluent USA; 2001.
9. Bezzo F, Macchietto S, Pantelides CC. A general framework for integration of computation fluid dynamics and process simulation. *Comput Chem Eng*. 2000;24:653-658.
10. Barton PI, Pantelides CC. Modeling of combined discrete/continuous processes. *AIChE J*. 1994;40:966-979.
11. Oh M, Pantelides CC. A modelling and simulation language for combined lumped and distributed parameter systems. *Comput Chem Eng*. 1996;20:611-633.
12. Bezzo F, Macchietto S, Pantelides CC. General hybrid multizonal/CFD approach for bioreactor modeling. *AIChE J*. 2003;49:2133-2148.
13. van der Molen TJ, van Heerden C. The effect of imperfect mixing on the initiator productivity in the high pressure radical polymerization of ethylene. Proc of 1st Int Symp on Chemical Reaction Engineering. Washington, DC: American Chemical Society; 1970.
14. Marini L, Georgakis C. The effect of imperfect mixing on polymer quality in low density polyethylene vessel reactors. *Chem Eng Commun*. 1984;30:361-375.
15. Marini L, Georgakis C. Low-density polyethylene vessel reactors. Part I: Steady state and dynamic modeling. *AIChE J*. 1984;30:401-408.
16. Marini L, Georgakis C. Low-density polyethylene vessel reactors. Part II: A novel controller. *AIChE J*. 1984;30:409-414.
17. Zhang SX, Ray WH. Modeling of imperfect mixing and its effects on polymer properties. *AIChE J*. 1997;43:1265-1277.
18. Villa CM, Dihora JO, Ray WH. Effects of imperfect mixing on low-density polyethylene reactor dynamics. *AIChE J*. 1998;44:1646-1656.
19. McCoy M, Reisch MS, Tullo AH, Short PL, Thayer AM, Tremblay JF, Storck WJ. Facts and figures for the chemical industry. *Chem Eng News*. 2003;81:25-66.

20. Beasley JK. Polymerization at high pressure. In: Allen SG, Bevington JC, eds. *Comprehensive Polymer Science*. New York, NY: Pergamon Press; 1989:273-282.
21. Gemassmer AM. Autoclave process for the high pressure polymerization of ethylene. *Erdöl Kohle Erdgas Petrochem*. 1978;31:221-228.
22. Christl RJ, Roedel MJ. Constant Environmental Process for Polymerizing Ethylene. U.S. Patent No. 2 897 183; 1959.
23. Pladis P, Kiparissides C. Steady-state multiplicity in high pressure ethylene polymerization reactors. Proc of 3rd Annual Polymer Producers Conference (AIChE), Houston, TX; 1999.
24. Donati G, Gramondo M, Langianni E, Marini L. Low density polyethylene in vessel reactors. *Q Ing Chim Ital*. 1981;17:88-96.
25. van der Molen TJ, Koenen A, Oosterwijk H, van der Bend H. "Light-off " temperature and consumption of 16 initiators in LDPE production. *Q Ing Chim Ital*. 1982;18:7-15.
26. Singstad P. *Modelling and Multivariable Control of High Pressure Autoclave Reactors for Polymerization of Ethene*. PhD Dissertation. Trondheim, Norway: The Norwegian Institute of Technology; 1992.
27. Read NK, Zhang SX, Ray WH. Simulations of a LDPE reactor using computational fluid dynamics. *AIChE J*. 1997;43:104-117.
28. Zhang SX, Read NK, Ray WH. Runaway phenomena in low-density polyethylene autoclave reactors. *AIChE J*. 1996;42:2911-2925.
29. Wells GJ. *Modeling Methods for Predicting Polymer Process Dynamics and Product Properties: The Effects of Mixing and Catalyst Characteristics*. PhD Dissertation. Madison, WI: University of Wisconsin; 2003.
30. Odian G. *Principles of Polymerization*. New York, NY: Wiley; 1991.
31. Chen CH, Vermeychuk JG, Howell JA, Ehrlich P. Computer model for tubular high-pressure polyethylene reactors. *AIChE J*. 1976;22:463-471.
32. Doak KW. Low density polyethylene. In: Mark HF, ed. *Encyclopedia of Polymer Science and Technology*. New York, NY: Wiley–Interscience; 1985:383-429.
33. Zhang SX. *Modelling and Experimental Studies of Free Radical Polymerization Reactors*. PhD Dissertation. Madison, WI: University of Wisconsin; 1996.
34. Yakhot V, Orszag SA. Renormalization group analysis of turbulence. I. Basic theory. *J Sci Comput*. 1986;1:3-51.
35. Launder BE, Spalding DB. The numerical computation of turbulent flows. *Comput Methods Appl Mech Eng*. 1974;3:269-289.
36. Young RJ, Lovell PA. *Introduction to Polymers*. London: Chapman & Hall; 1991.
37. Tosun G, Bakker A. A study of macrosegregation in low-density polyethylene autoclave reactors by computational fluid dynamic modeling. *Ind Eng Chem Res*. 1997;36:296-305.
38. Fox RO. On the relationship between Lagrangian micromixing models and computational fluid dynamics. *Chem Eng Process*. 1998;37:521-535.
39. Fox RO. *Computational Models for Turbulent Reacting Flows*. Cambridge, UK: Cambridge Univ. Press; 2003.
40. Baldyga J, Bourne JR. A fluid mechanical approach to turbulent mixing and chemical reaction—Part I: Inadequacies of available methods. *Chem Eng Commun*, 1984;28:231-241.
41. Baldyga J, Bourne JR. A fluid mechanical approach to turbulent mixing and chemical reaction—Part II: Micromixing in the light of turbulence theory. *Chem Eng Commun*. 1984;28:243-258.
42. Baldyga J, Bourne JR. A fluid mechanical approach to turbulent mixing and chemical reaction—Part III: Computational and experimental results for the new micromixing model. *Chem Eng Commun*. 1984;28:259-281.
43. Villermaux J, Pons M, Blavier L. Comparison of partial segregation models for the determination of kinetic constants in a high pressure polyethylene reactor. Proc of 8th Int Symp on Chemical Reaction Engineering. Edinburgh, Scotland: Pergamon Press; 1984.
44. Baldyga J, Bourne JR, Hearn SJ. Interaction between chemical reactions and mixing on various scales. *Chem Eng Sci*. 1997;52:457-466.
45. Levenspiel O. *Chemical Reaction Engineering*. New York, NY: Wiley; 1999.
46. Tabis B, Essekkat A. Three-phase multicompartment model for fluidized-bed catalytic reactors: Autothermicity and multiplicity of steady states. *Chem Eng Sci*. 1992;47:407-419.
47. Georgakis C, Marini L. The effect of mixing on steady-state and stability characteristics of low density polyethylene vessel reactors. Proc of 7th Int Symp on Chemical Engineering. Boston, MA: American Chemical Society; 1982.
48. Chan WM, Gloor PE, Hamielec AE. A Kinetic model for olefin polymerization in high-pressure autoclave reactors. *AIChE J*. 1993;39:111-126.
49. Pladis P, Kiparissides C. Dynamic modeling of multizone, multifeed high-pressure LDPE autoclaves. *J Appl Polym Sci*. 1998;73:2327-2348.
50. Enfors SO, Jahic M, Rozkov A, Xu B, Hecer M, Jürgen B, Krüger E, Schweder T, Hamer G, O'Beirne D, Noisommit-Rizzi N, Reuss M, Boone L, Hewitt C, McFarlane C, Nienow A, Kovacs T, Trägårdh C, Fuchs L, Revstedt J, Friberg PC, Hjertager BH, Blomsten G, Skogman H, Hjort S, Hoeks F, Lin HY, Neubauer P, van der Lans RGJM, Luyben KCAM, Vrábel P, Manelius Å. Physiological responses to mixing in large scale bioreactors. *J Biotechnol*. 2001;85:175-185.
51. Shah JJ, Fox RO. Computational fluid dynamics simulation of chemical reactors: Application of in situ adaptive tabulation to methane thermochlorination chemistry. *Ind Eng Chem Res*. 1999;38:4200-4212.
52. Raman V, Fox RO, Harvey AD, West DH. CFD analysis of premixed methane chlorination reactors with detailed chemistry. *Ind Eng Chem Res*. 2001;40:5170-5176.
53. Wells GJ, Ray WH. Mixing effects on performance and stability of low-density polyethylene autoclave reactors. *AICHE J*. 2005 in press.
54. Nowak U, Weimann L. A family of Newton codes for systems of highly nonlinear equations. Zuse Institute, Berlin. Technical Report TR-91-10. 1991.
55. Doedel E. AUTO: A program for the automatic bifurcation analysis of autonomous systems. *Congres Numer*. 1981;30:265-284.
56. Petzold LR. Description of DASSL: A differential/algebraic system solver. Sandia National Lab. Technical Report SAND82-8637; 1982.
57. Wells GJ, Ray WH. Prediction of molecular weight distribution in low-density polyethylene reactors. *Macromolecular Materials and Eng*. 2005;209:319-346.
58. Versteeg HK, Malalasekera W. *An Introduction to Computational Fluid Dynamics. The Finite Volume Approach*. London: Longman Group; 1995.

Appendix

The state equations for zone k of a compartment model are given below. If not specified, all rate constants, concentrations, mass fractions, and temperatures are at the conditions of the compartment k. Compartment volumes are assumed to be time invariant, and constant physical properties are also assumed.

$$\frac{dw_I^k}{dt} = \frac{1}{\rho V_k}\sum_{n=0}^{N_{compt}} f_n^k Q_n w_I^n - k_d C_I \frac{MW_I}{\rho} \tag{A1}$$

$$\frac{d\mu_0^k}{dt} = \frac{1}{V_k}\sum_{n=0}^{N_{compt}} f_n^k \frac{Q_n}{\rho_n}\,\mu_0^n + 2k_d f_{eff} C_I - k_{tc}(\mu_0)^2 \tag{A2}$$

$$\frac{dw_p^k}{dt} = \frac{1}{\rho V_k}\sum_{n=0}^{N_{compt}} f_n^k Q_n w_p^n + \frac{k_p C_{mon}\mu_0 MW_{mon}}{\rho} \tag{A3}$$

$$\frac{dT^k}{dt} = \frac{1}{\rho V_k}\sum_{n=0}^{N_{compt}} f_n^k Q_n T^n - \left\{\frac{\Delta H_{poly} k_p C_{mon}\mu_0}{\rho C_p}\right\} - \left\{\frac{\Delta H_{decomp}\left[C_{mon}^2(1.89k_{md} + k_{pdl}) + 0.0714k_{pd2}C_{mon}\right]}{\rho C_p}\right\} \tag{A4}$$

Manuscript received Apr. 8, 2004, and revision received Sept. 10, 2004.